FIRST SOLAR EUV IRRADIANCES OBTAINED FROM SOHO BY THE CELIAS/SEM*

D. L. JUDGE, D. R. McMULLIN and H. S. OGAWA
Department of Physics and Astronomy and Space Sciences Center, University of Southern California, Los Angeles, CA 90089-1341, U.S.A.

D. HOVESTADT, B. KLECKER and M. HILCHENBACH
Max-Planck Institut für extraterrestrishe Physik, D-85740 Garching, Germany

E. MÖBIUS
University of New Hampshire, Durham, New Hampshire 03824-3525, U.S.A.

L. R. CANFIELD, R. E. VEST, R. WATTS and C. TARRIO
Physics Laboratory, National Institute of Standards and Technology, Gaithersburg, MA 20899, U.S.A.

M. KÜHNE
Physikalisch-Technische Bundesanstalt, D-10587 Berlin, Germany

P. WURZ
Physikalisches Institut, University of Bern, 3012 Bern, Switzerland

(Received 3 December 1996; accepted 8 January 1997)

Abstract. The first results obtained with the Solar EUV Monitor (SEM), part of the Charge, Element, and Isotope Analysis System (CELIAS) instrument, aboard the SOlar and Heliospheric Observatory (SOHO) satellite are presented. The instrument monitors the full-disk absolute value of the solar He II irradiance at 30.4 nm, and the full-disk absolute solar irradiance integrated between 0.1 nm and 77 nm. The SEM was first turned on December 15, 1995 and obtained 'first light' on December 16, 1995. At this time the SOHO spacecraft was close to the L-1 Lagrange point, 1.5×10^6 km from the Earth towards the Sun. The data obtained by the SEM during the first four and a half months of operation will be presented. Although the period of observation is near solar minimum, the SEM data reveal strong short-term solar irradiance variations in the broad-band, central image channel, which includes solar X-ray emissions.

1. Introduction

The Solar EUV Monitor (SEM) is a highly stable transmission grating solar extreme ultraviolet (EUV) spectrometer that is integrated into the Charge, Element, and Isotope Analysis System (CELIAS) instrument which measures the mass, ionic charge, and energy of the low- and high-speed solar wind, suprathermal ions, and low energy solar flare particles (Hovestadt *et al.*, 1995). The SEM solar irradiance data will not only supplement the CELIAS helium pick-up ion data by providing the ionization rate of inflowing interstellar neutral helium atoms, but will also provide a reliable solar flux data base for inter-calibration of the Extreme ultraviolet

* Paper presented at the SOLERS22 International Workshop, held at the National Solar Observatory, Sacramento Peak, Sunspot, New Mexico, U.S.A., June 17–21, 1996.

J. M. Pap et al. (eds.), *Solar Electromagnetic Radiation Study for Solar Cycle 22*

Table I
Uncertainty (1σ) in CELIAS/SEM flux measurements

Uncertainty component	First-order (channel 1 and 3) Relative uncertainty (%)	Zero-order (channel 2) Relative uncertainty (%)
SURF BL-9 monochromatic flux measurement	5.0	5.0
SEM calibration repeatability	0.1	0.1
SEM counting statistics	0.1	0.1
SEM pointing accuracy	1.5	0.3
Electronics stability (1 yr)	1.0	1.0
Grating stability (1st yr)[a,b]	2.5	2.5
Filter stability (1st yr)[a]	5.0	5.0
Detector stability (1st yr)[a]	5.0	5.0
Theoretical modeling of sensitivity below 5.0 nm[c]	0.7	5.0
Relative solar spectral distribution	10.0	10.0
Relative combined standard uncertainty (1σ) (%)	13.6	14.4

[a] Calibration may change due to contamination by outgassing products and damage from solar wind, dust particles, and cosmic rays. First year stability is dominated by pre-launch handling and storage in the Earth's atmosphere. In subsequent years, the CELIAS/SEM stability will be determined by filter and detector stability, but at significantly lower uncertainty. The true stability of the instrument will be determined by sounding rocket underflights.
[b] Calibration may change due to unexpected mechanical stresses during launch and during initial thermal cycling. Since the aperture cover was permanently removed on December 16, 1995, the CELIAS/SEM has been thermally stable. Periodic sounding rocket underflight recalibration of the CELIAS/SEM will determine any calibration changes which may have occurred during instrument integration, launch, and/or orbit operation.
[c] The first-order channels are nominally insensitive to multiple-order short-wavelength radiation (<1% of the measured signal) using the solar spectrum adopted here. However, in principle, larger signals can be expected in the 30.4 nm band when strong soft X-ray emissions are present.

Imaging Telescope (EIT), Coronal Diagnostic Spectrometer (CDS), Solar Ultraviolet Measurements of Emitted Radiation (SUMER), and Ultra-Violet Coronograph Spectrometer (UVCS) instruments aboard the SOlar and Heliospheric Observatory (SOHO) (Domingo and Guynne, 1989). Furthermore, the SEM data base is nearly continuous in time, providing the first long-term solar EUV data using a spectrometer specifically designed to be highly stable throughout an extended mission. The data will not only be of interest to the SOHO investigators but will also be of great interest to aeronomers who are investigating both the dynamics and steady-state properties of planetary atmospheres.

About a decade ago, freshly ionized interstellar He pick-up ions in the solar wind were measured by means of a time-of-flight spectrometer (Möbius *et al.*,

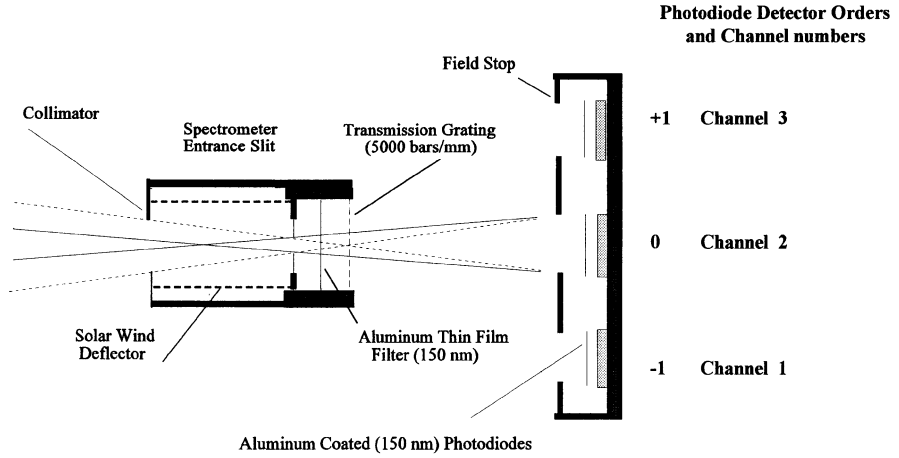

Figure 1. Schematic diagram of the CELIAS/SEM components and optics.

1985). This new technique provided a method of studying the state of the local interstellar medium complementary to the techniques employing backscattering of solar ultraviolet radiation (Holzer, 1977). The flux of pick-up ions in the solar wind depends on the product of the local neutral atom density and the ionization rate of the inflowing neutral gas. Since the ionization rate can only be determined indirectly from the particle measurements, an independent, absolute measurement of this quantity by the SEM significantly improves the accuracy of the local interstellar medium characterization.

Another SEM objective is to provide a stable, full-disk irradiance monitor whose data can be compared with the full-disk 30.4 nm irradiance measurements of EIT and full-disk irradiance measurements by CDS. Once the comparison is made, the calibration can be transferred to SUMER and UVCS in the overlapping wavelength regions.

Interest by the aeronomy community in the solar EUV data arises from the fact that the solar EUV flux at wavelengths less than 100 nm is deposited in planetary atmospheres, and is highly variable with solar activity (Lean, 1990). It produces heating, ionization, and excitation of atomic and molecular species, thus leading to complex chemical and transport processes in the affected atmospheric regions. By combining the absolute flux measurements obtained by the SEM with the spectral distributions obtained by CDS (15–80 nm), UVCS (50–126 nm), and SUMER (50–160 nm), it is possible to infer the absolute amount of energy being deposited at various altitudes in, for example, the Earth's atmosphere. Such data are extremely valuable since most of the energy in the spectral regime between 0.1 nm and 77 nm (measured by the undiffracted zero-order channel of the SEM) is deposited in the thermosphere, although a significant fraction can penetrate still deeper into the atmosphere because of rapidly decreasing absorption cross-sections of atmospheric

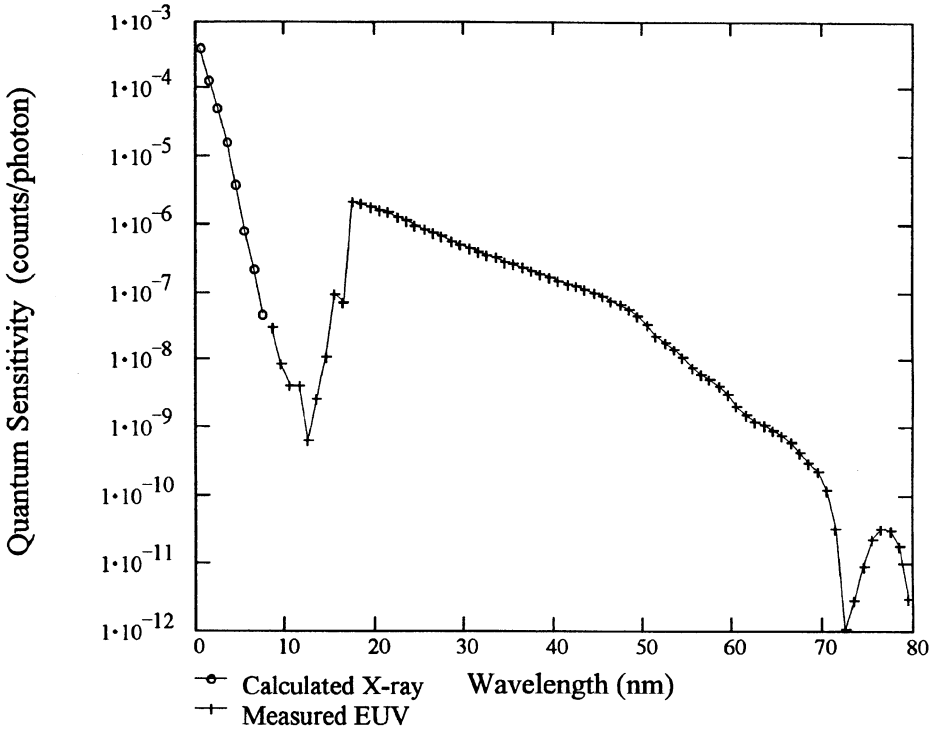

Figure 2. The CELIAS/SEM quantum sensitivity, in counts/photon, as a function of wavelength. The sensitivity was measured at NIST, Gaithersburg, MD, U.S.A. from 5 to 80 nm. The quantum efficiencies of the aluminum coated Si diodes along with the transmission of our free-standing Al filter for wavelengths between 0.1 and 12.3 nm were calculated by Loren Acton of Montana State University from the thickness and optical properties of Si, SiO_2, Al, and Al_2O_3. This figure shows calculated values from 0.1 to 6.5 nm and measured values from 6.5 to 80 nm.

gases in the soft X-ray regime (Barth *et al.*, 1988). The SEM data will also help resolve a number of open questions and discrepancies concerning the interaction of solar EUV radiation with the upper atmosphere. One such open question is a discrepancy between the measured photoelectron flux in the ionosphere and the observed solar EUV flux which produces it (Richards and Torr, 1984, 1988; Richards, Fennelly, and Torr, 1994).

2. Instrumentation

The SEM is a simple transmission grating spectrometer and makes use of state-of-the-art technology in the EUV wavelength region (Ogawa *et al.*, 1993; Hovestadt *et al.*, 1995). Briefly, it is a lightweight (480 g) instrument that consists of a high-density transmission grating (5000 bars mm^{-1}) fitted with a free-standing aluminum filter immediately behind the SEM entrance aperture. A schematic dia-

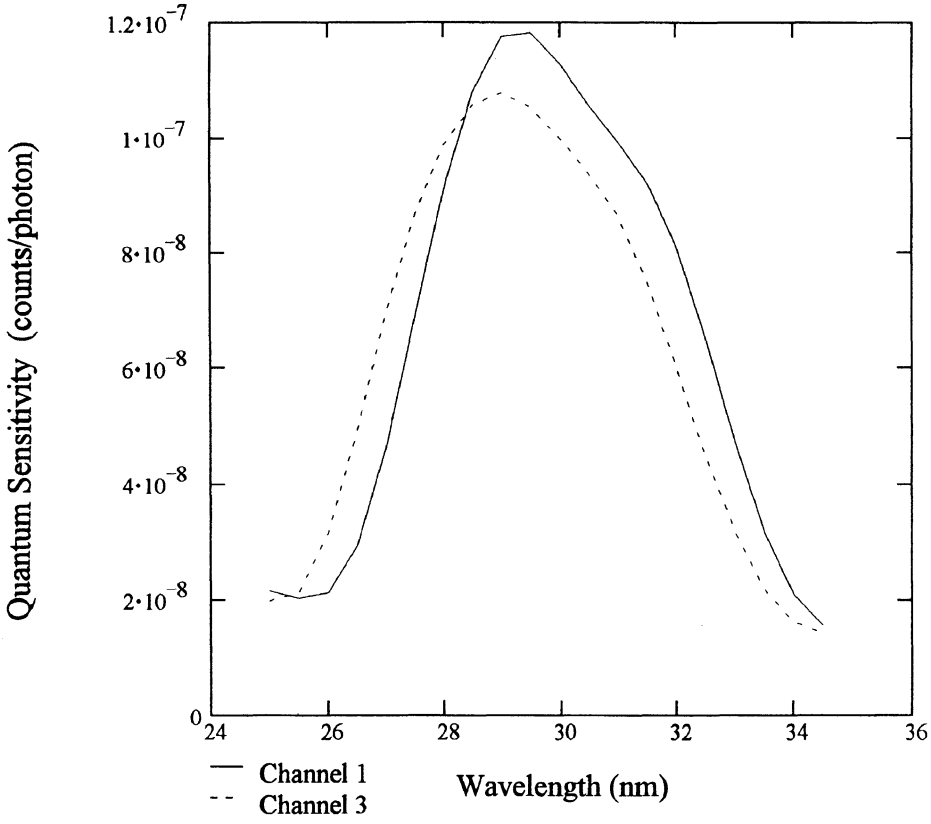

Figure 3. CELIAS/SEM first-order channel sensitivities, in count/photon, as a function of wavelength. Sensitivities were measured at NIST.

gram of the SEM is shown in Figure 1. Baffles (not shown) placed behind the grating are utilized to reduce scattered radiation. Any potential degradation of the aluminum filter from solar wind particles is minimized by solar wind deflector plates placed in front of the SEM entrance aperture. The aluminum film reduces the heat load on the grating and limits the wavelength range to the aluminum transmission region. The dispersed light is detected by three highly efficient, aluminum coated silicon photodiodes located 200 mm behind the grating at the zero-order and 30.4 nm first-order positions. The zero-order detector (channel 2) primarily measures the solar irradiance within the nominal aluminum bandpass (17–77 nm). However, due to the high sensitivity of silicon photodiodes and transmission of aluminum at short wavelengths, the zero-order channel also detects solar X-rays shortward of approximately 12.5 nm. The first-order detectors (channels 1 and 3) measure the irradiance within an 8 nm bandpass centered about the 30.4 nm solar He II emission and are nominally insensitive to soft X-rays (see Table I, footnote c).

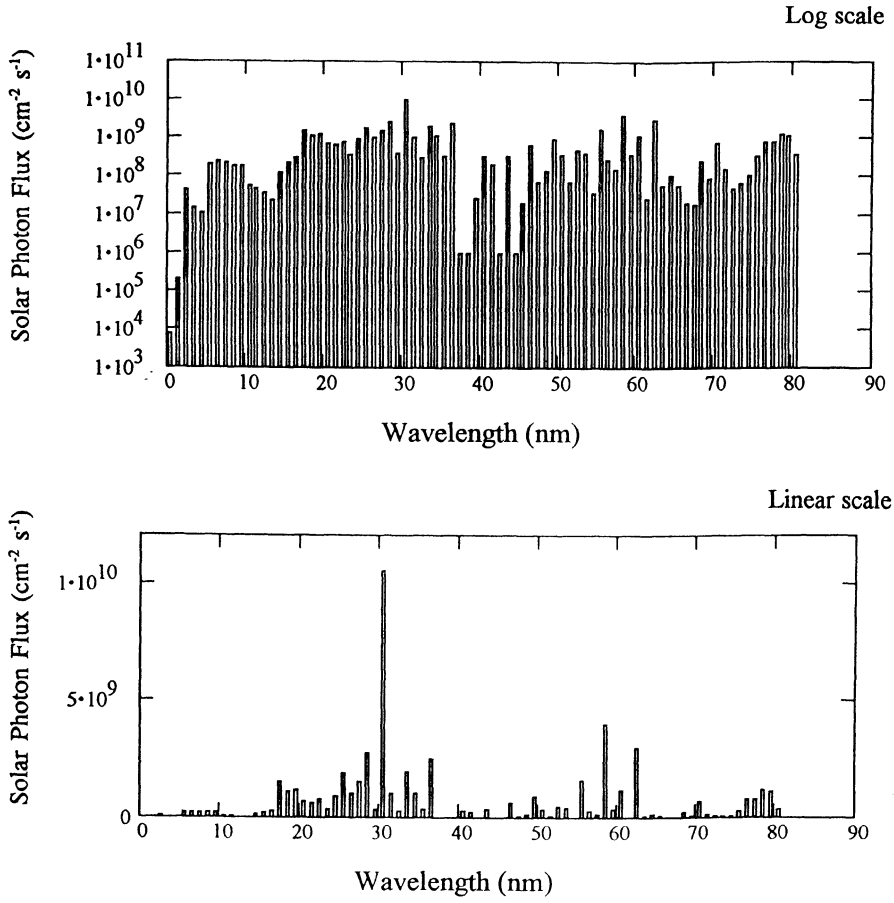

Figure 4. A composite solar photon flux distribution (cm^{-2} s^{-1}) in 1 nm bins between 0.1 and 80 nm. The upper panel is a log plot while the lower is linear. The spectrum is composed of data in different wavelength ranges taken under varying solar activity conditions: 0.1 to 0.8 nm, $F_{10.7} = 70$; 1 to 5 nm, $F_{10.7} = 127$; 5 to 80 nm, $F_{10.7} = 158$. This solar spectral distribution was adopted by the SOLERS22 Workshop held in Sacramento Peak, New Mexico in June 1996 as a zero-order approximation to a solar-minimum reference spectrum from the soft X-ray region through the EUV.

3. Calibration

The SEM was calibrated at SURF II (Furst *et al.*, 1995; Canfield, 1987) at the National Institute of Standards and Technology (NIST) in Gaithersburg, Maryland, U.S.A. The individual components of the SEM were first calibrated separately, and then the instrument as a whole was calibrated in both monochromatic radiation (on beamline 9) and in undispersed synchrotron radiation (on beamline 2). The calibration constant of the current-to-frequency conversion electronics, the transmission of the grating (25.5, 30.4, and 33.5 nm), the quantum yield of the aluminum coated photodiodes (5–80 nm), and the transmission of the free-standing alumin-

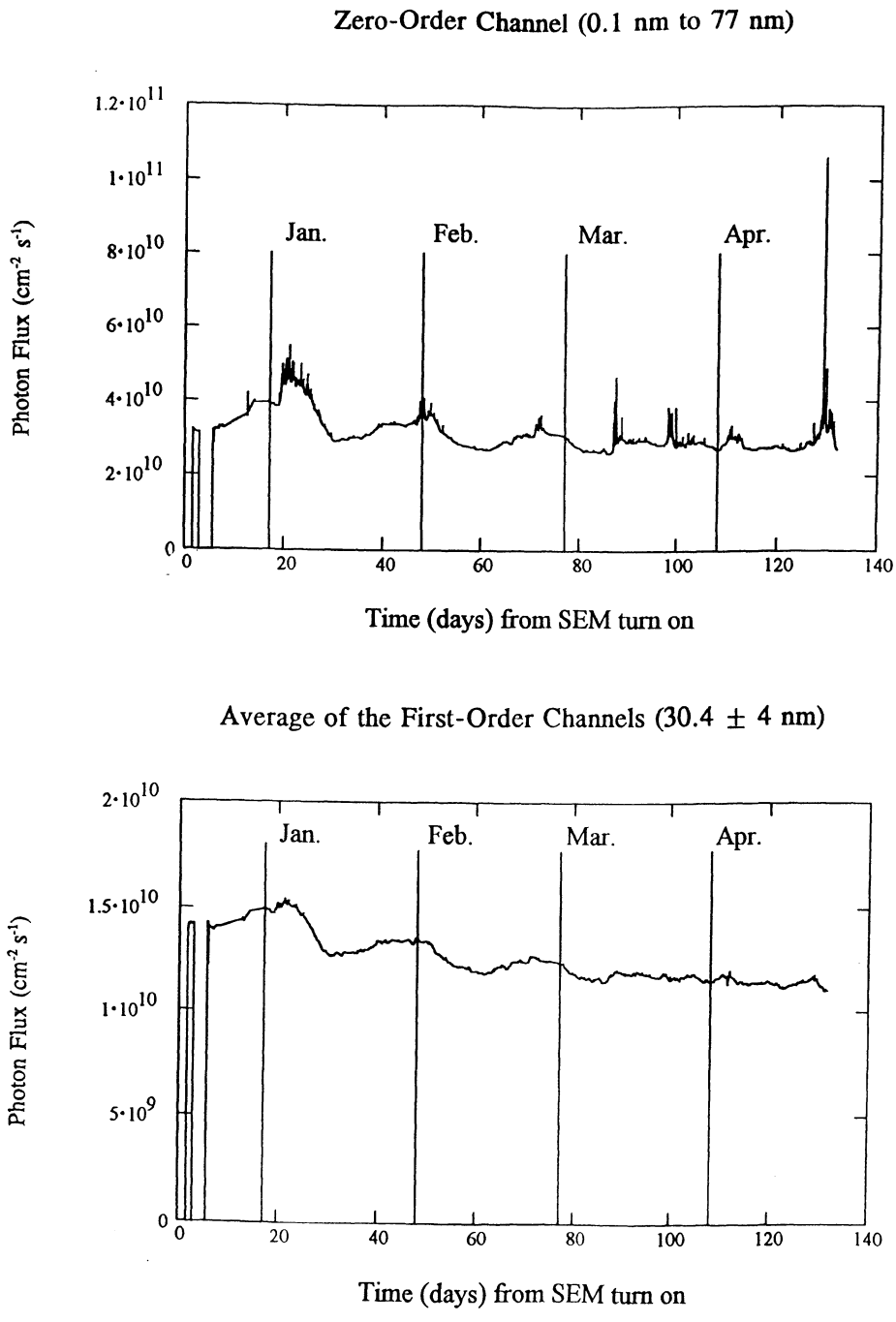

Figure 5. 'First light' zero- and first-order CELIAS/SEM photon fluxes ($cm^{-2}\ s^{-1}$) plotted for a $4\frac{1}{2}$ month period. The background has been subtracted and the data were averaged over 10 min. The hash and spikes in the zero-order channel are real variations in solar flux. Time $t = 0$ is on December 15, 1995 when the SEM instrument was first turned on, but with the solar viewing aperture blocked. The SEM aperture cover was permanently removed on December 16, 1996, providing the first light data for about one day as shown. The SEM was turned off again for a few days during CELIAS outgassing.

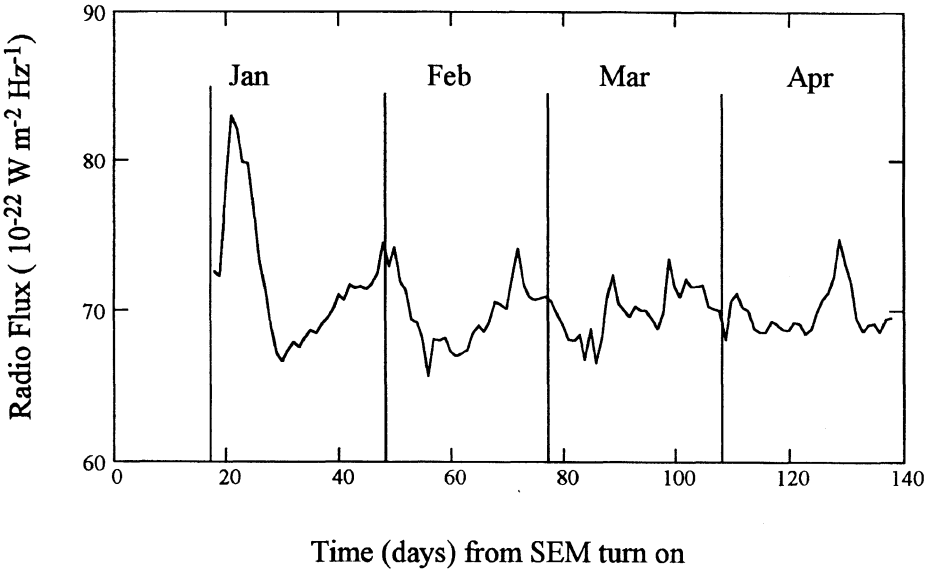

Figure 6. $F_{10.7}$ radio flux density at 28 MHz adjusted to a distance of 1.5×10^8 km from the Sun plotted against time for comparison with the CELIAS/SEM data.

um filter (5–80 nm) were measured independently. The 'end to end' calibration in monochromatic radiation is the most accurate of the three methods used, and is the calibration considered in the remainder of this discussion. The combined component efficiency agrees with the 'end to end' calibration of the whole instrument to within 5%, well within the combined uncertainty of the measurements. The instrument sensitivity at the time of calibration, approximately one year before launch, is presented in Figures 2 and 3 for the zero-order and first-order channels, respectively. The zero-order quantum sensitivity has been extended shortward of the measured calibration (6.5 to 80.0 nm) to 0.1 nm by theoretical modeling using the thickness and optical properties of silicon, silicon dioxide, aluminum, and aluminum oxide between 0.1 and 6.5 nm (L. Acton, 1996, priv. comm.).

The uncertainty of the flux measurements (all uncertainties given in this paper are standard uncertainties stated as 1σ) provided by the SEM depends on both the calibration uncertainty and the stability of the optical components over time. Both types of uncertainty are summarized in Table I, and the uncertainty of the SEM absolute solar flux measurements is calculated as the sum in quadrature of the uncertainty components. The stability figures presented in Table I include the effects of pre-launch handling and storage in the Earth's atmosphere. On-orbit stability should be much improved over the first year value. The calculation of photon flux, particularly for the broad-band zero-order channel, depends on the relative solar spectrum that produces the measured photocurrent. The first-order channels are sensibly unaffected by the short wavelength sensitivity modeling because they are

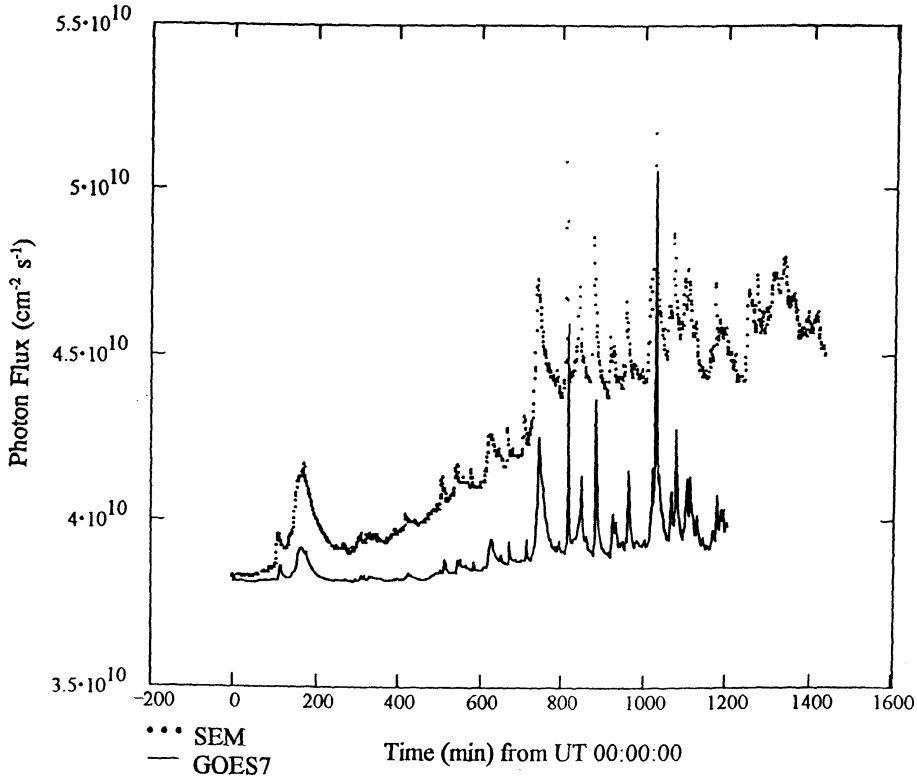

GOES flux scaled according to 1.2×10^{16} flux (W m^{-2}) + 3.8×10^{10}.

Figure 7. One-minute averages of the zero-order CELIAS/SEM photon flux (cm^{-2} s^{-1}) with the background subtracted and plotted against time for January 3, 1996. The GOES-7 one-minute averages have been scaled and plotted for comparison. The zero-order SEM channel is not only sensitive to the nominal 17 to 77 nm aluminum bandpass, but also to the 0.1 to 12.5 nm solar soft X-rays, where the transmission of aluminum rises and the diode detection efficiency is high.

Table II
Instrument sensitivy range and first light absolute intensity

	First order (channels 1 and 3)	Zero order (channel 2)
Wavelength range (nm)	25–34	0.1–77
Photon flux (cm^{-2} s^{-1})	$(1.38 \pm 0.19) \times 10^{10}$ (1σ)	$(3.16 \pm 0.44) \times 10^{10}$ (1σ)

nominally insensitive to radiation outside the 8 nm band centered at 30.4 nm in the absence of strong X-ray bursts.

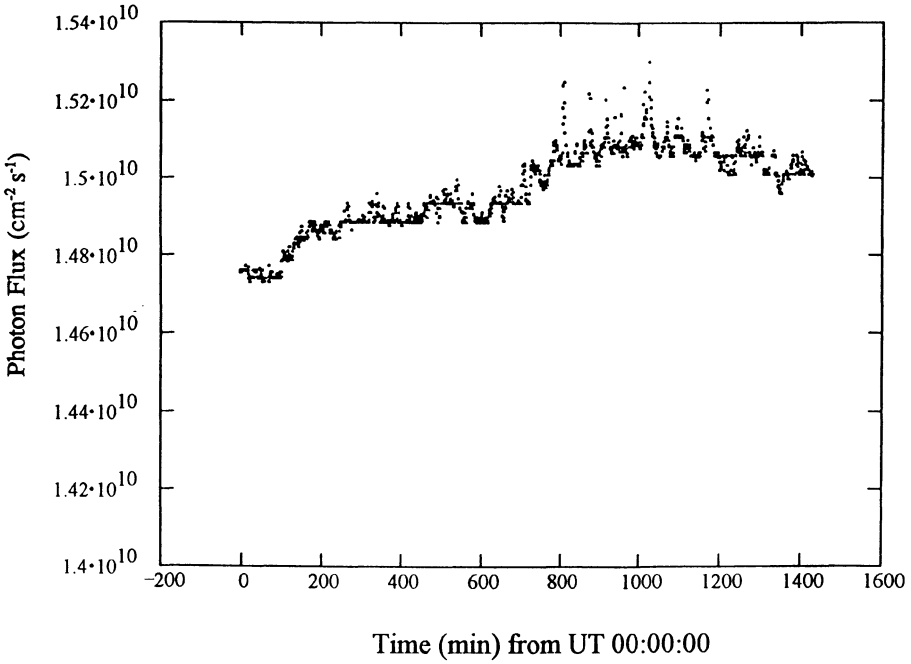

Figure 8. The CELIAS/SEM first-order photon flux measurements (cm^{-2} s^{-1}) are averaged and plotted against time over the same period as Figure 7. The first-order channels are nominally insensitive to the 0.1 to 12.5 nm soft X-rays. The modest increases at 30.4 nm are real and accompany the increases in the solar soft X-ray wavelength region.

4. Results

Note that the value of absolute solar flux that we report is directly dependent on the accuracy of the full-disk relative solar-spectral distribution within the bandpass of each channel. Presently, a simultaneous full-disk spectral distribution within the bands of interest during the SOHO mission is not available. Therefore, we have used earlier data to produce the full-disk composite spectmm between 0.1 and 80 nm, shown in Figure 4 (Freeman and Jones, 1970; Kreplin and Horan, 1992; Van Tassel, McMahon, and Héroux, 1981). It should be mentioned, however, that an improved fit to the altitude profile data obtained by instrumentation onboard the SOHO underflight calibration rocket (June 26, 1996 White Sands Missile Range, New Mexico, flight 36.147) was obtained when the poorly known solar flux shortward of 5 nm shown in Figure 4 was increased by a factor of five. This flux increase contributes only to the zero-order signal and changes the total flux in the composite spectrum between 0.1 and 77 nm by less than 1%. When simultaneous relative fluxes do become available throughout the wavelength range of interest, we will reevaluate our results. With these caveats, the 'first light' absolute photon fluxes at

L-1 obtained by the SEM are presented in Table II. These flux values reflect the most recent inflight recalibration of the SOHO CELIAS/SEM instrument.

The SEM data obtained during the first $4\frac{1}{2}$ months of operation are shown in Figure 5. The zero- and first-order absolute photon fluxes (10 min averages) are plotted against time. Time $t = 0$ is when the SEM was first turned on (December 15, 1995). For comparison, the $F_{10.7}$ radio flux is plotted in Figure 6 on the same time scale as the SEM data. The SEM commissioning schedule is given below to provide a perspective on the instrument time line:

December 2, 1995		SOHO launched;
December 15, 1995	04:07 UT	SEM turn on (measuring dark count rates);
December 16, 1995	19:10 UT	SEM cover off (first light);
December 18, 1995	01:34 UT	SEM turned off (for CELIAS outgassing);
December 20, 1995	17:35 UT	SEM turned back on.

Since January 1996 the SEM has been continuously operating, relaying data through the Deep Space Network with 97% of all data relayed to ground stations.

Both the zero-order and first-order channels observed an increase in signal corresponding to an X-ray event on the Sun beginning on January 3, 1996. This event, as observed by the zero-order channel, is correlated with the GOES 7 (0.1–0.8 nm) data base (correlation coefficient = 1). While the first-order channels are very insensitive to X-rays, both the zero- and first-order channels show a 26-day variation in the observed flux. On April 22, 1996 an M-class flare erupted and was observed by the zero-order channel. It lasted for about 16 min. (The smallest integration time of the SEM is 15 s.) The GOES 7 X-ray data show an increase by a factor of 100 for about 12 min. The longer period observed by the SEM indicates that it is measuring soft X-rays in addition to the hard X-rays also seen by GOES 7. The SEM zero-order channel (15 s integration) data show a factor of 5 increase in signal indicating a photon flux as large as that of Lα (3.0×10^{11} ph cm^{-1} s^{-1}) (Tobiska, 1996, priv. comm.) and an energy increase of at least a factor of ten greater than Lα, assuming an average photon wavelength of 10.0 nm.

In Figure 7, the 1 min zero-order SEM averages are plotted against time on January 3, 1996. For comparison, we also plot the GOES7 (0.1–0.8 nm) 1 min averages scaled to the SEM photon flux. The SEM first-order channel data have been averaged and plotted on the same time scale in Figure 8. A complete understanding of the EUV temporal evolution of the EUV and X-ray flux requires full-disk solar spectral data throughout the wavelength range of interest. The highly varying components shown in Figure 7 (short-term variation of the order of an hour), and in the 30.4 nm channel in Figure 8, indicate that enhanced EUV emission accompanies X-ray emission events.

5. Summary

The full-disk solar EUV data obtained by the SEM instrument aboard SOHO are of excellent quality and show significant EUV variability even though the observations are near solar minimum. We have obtained and presented $4\frac{1}{2}$ months of nearly continuous data (10 min averages) from December 16, 1995 through April 26, 1996. During this near solar minimum period of solar cycle 22, an active region appeared on the east limb of the Sun on January 3, 1996, and persisted throughout the next several months, as may be seen in the 26-day modulation of the solar flux measured in all three SEM channels. An M-class flare was observed on April 22, 1996 both by GOES 7 in the 0.1 to 0.8 nm wavelength range and in the zero-order SEM channel. The short-term solar flux variation measured during the solar flare flash phase is much larger in amplitude than the short-term variations observed during the January 3, 1996 X-ray event. During both events, the short-term variations were measured in the SEM zero-order and first-order channels. The first-order channels, however, showed variations of much smaller amplitude.

Acknowledgements

This work is supported by NASA grant NAG5–5018. The $F_{10.7}$ radio flux data are provided as a service of the National Research Council of Canada. We wish to thank Mitch Furst and Rossie Graves of NIST for their invaluable assistance in carrying out the white-light calibration at SURF II. We are also grateful to Loren Acton of Montana State University for his many helpful discussions, for providing the GOES 7 X-ray data, and for his computation of the silicon photodiode detector efficiencies and aluminum filter transmission shortward of 12.3 nm.

References

Acton, L.: 1996, private communication.
Barth, C. A., Tobiska, W. K., Siskind, D. E., and Cleary, D. D.: 1988, *Geophys. Res. Letters* **15**, 92.
Canfield, L. R.: 1987, *Appl. Optics* **26**, 3831.
Domingo, V.: 1989, in T. D. Guyenne (ed.), ESA SP-1104.
Freeman, F. F. and Jones, B.B.: 1970, *Solar Phys.* **15**, 288.
Furst, M. L., Graves, R. M., Canfield, L. R., and Vest, R. E.: 1995, *Rev. Sci. Instrum.* **66**, 2257.
Holzer, T. E.: 1977, *Geophys. Space Phys.* **15**, 467.
Hovestadt, D., Hilchenbach, M., Bürgi, A., Klecker, B., Laeverenz, P., Scholer, M., Grunwaldt, H, Axford, W. I., Livi, S., Marsch, E., Wilken, B., Winterhoff, H. P., Ipavich, F. M., Bedini, P., Coplan, M. A., Galvin, A. B., Gloeckler, G., Bochsler, P., Balsiger, H., Fischer, J., Geiss, J., Kallenbach, R., Wurz, P., Reiche, K.-U., Gliem, F., Judge, D. L., Ogawa, H. S., Hsieh, K. C., Möbius, E., Lee, M. A., Managadze, G. G., Verigin, M. I., and Neugebauer, M.: 1995, *Solar Phys.* **162**, 441.
Kreplin, R. W. and Horan, D. M.: 1992, in R. F. Donnelly (ed.), *Proceedings of the Workshop on the Solar Electromagnetic Radiation Study for Solar Cycle 22*, p. 405.
Lean, J.: 1990, *J. Geophys. Res.* **95** (A8), 11933.

Möbius, E., Hovestadt, D., Klecker, B., Scholer, M., Gloeckler, G., and Ipavich, F. M.: 1985, *Nature* **318**, 426.
Ogawa, H. S., McMullin, D. R., Judge, D. L., and Korde, R.: 1993, *Optical Eng.* **32**, 3121.
Richards, P. G. and Torr, D. G.: 1984, *J. Geophys. Res.* **89**, 5625.
Richards, P. G. and Torr, D. G.: 1988, *J. Geophys. Res.* **93**, 4060.
Richards, P. G., Fennelly, J. A., and Torr, D. G.: 1994, *J. Geophys. Res.* **99**, 8981.
Tobiska, W. K.: 1996, private communication.
Van Tassel, R. A., McMahon, W. J., and Héroux, L.: 1981, AFGL-TR-81-0111, Res. pap. 737.